Available online at www.CivileJournal.org

Civil Engineering Journal

(E-ISSN: 2476-3055; ISSN: 2676-6957)

Vol. 11, No. 08, August, 2025

Influence of Blast Furnace Slag on Concrete: Mechanical Strength and Microstructural Characterization

Edgar Yurihuaman [1], Gonzalo Cordova [1], Christhian Benavente [1], Anjhinson Romero [1*]

[1] *Professional School of Civil Engineering, San Juan Bautista Private University, Chincha 11702, Peru.*

Received 10 April 2025; Revised 21 July 2025; Accepted 28 July 2025; Published 01 August 2025

Abstract

This study aims to quantitatively assess the effect of granulated blast furnace slag (GGBFS) as a partial replacement for Portland cement on the mechanical and microstructural performance of concrete with a design compressive strength of 280 kg/cm². A comprehensive experimental program was conducted to evaluate compressive strength, indirect tensile strength, flexural strength, and modulus of elasticity at curing ages of 7, 14, and 28 days, in accordance with ASTM standards. Microstructural characterization included Fourier Transform Infrared Spectroscopy (FTIR), Scanning Electron Microscopy with Energy-Dispersive X-ray Spectroscopy (SEM/EDS), and X-ray Diffraction (XRD). The results demonstrated that incorporating GGBFS, particularly at 16% and 20% replacement levels, led to significant improvements in compressive strength and stiffness at 28 days, while early-age tensile strength reductions were mitigated over time due to the latent pozzolanic activity of the slag. Microstructural analyses revealed a denser cementitious matrix, enhanced chemical stability, and the formation of new crystalline phases. Statistical analyses (ANOVA and Kruskal–Wallis) confirmed significant effects on flexural strength and elastic modulus. These findings underscore the potential of GGBFS to improve concrete performance and promote sustainability by valorizing industrial by-products and reducing CO_2 emissions. This work provides a robust experimental and analytical basis for optimizing GGBFS incorporation in durable, performance-enhanced concretes.

Keywords: GGBFS; Blast Furnace Slag; Mechanical Properties; Microstructural Characteristics.

1. Introduction

Concrete is one of the most important construction materials worldwide [1–3], whose versatility and relative cost-effectiveness have made it a fundamental component of modern infrastructure [4–6]. Due to its broad range of applications, global concrete consumption has reached approximately 15 billion tonnes annually [7, 8]. However, concrete production—particularly that of its main binder, cement—has significant environmental impacts due to its high energy demand and the substantial greenhouse gas (GHG) emissions associated with its manufacture [9]. Currently, global cement production stands at around 4.2 billion tonnes per year and is projected to reach 5.5 billion tonnes by 2050 [10].

In terms of global demand, cement is among the most widely used substances, playing a critical role in infrastructure, buildings, and transportation systems [11]. Consequently, it is expected to remain central to the sustainable development of society in the coming decades [12–14]. The construction sector accounts for approximately 40% of global energy consumption and 30% of total natural resource depletion, while contributing nearly 40% of global CO_2 emissions and around 30% of solid waste generation [15]. Estimates suggest that between 4% and 9% of global CO_2 emissions are

* Corresponding author: 2020001165@unfv.edu.pe

http://dx.doi.org/10.28991/CEJ-2025-011-08-01

directly attributable to cement manufacturing [16, 17], primarily due to the decarbonation of $CaCO_3$ to CaO and the energy required for production and transportation [18]. Currently, emissions from cement plants account for over 5% of total global emissions [19], with the production of one tonne of cement generating approximately 0.95 tonnes of CO_2, thereby posing additional negative impacts on both human health and the environment [20].

In this context, the growing demand for more durable and sustainable structures has driven the search for and development of supplementary cementitious materials (SCMs) that enhance concrete performance while reducing its carbon footprint [21, 22]. One of the most effective strategies is the partial or total replacement of ordinary Portland cement (OPC) with SCMs [23, 24], including ground granulated blast furnace slag (GGBFS), fly ash, and silica fume [25]. These materials contribute to improved strength and durability, enhance workability, and reduce the carbon emissions associated with concrete production [26, 27]. Accordingly, clinker substitution with SCMs is widely recognized as one of the most effective and viable approaches, considering their availability and technical performance [28]. Moreover, the use of GGBFS significantly reduces CO_2 emissions per tonne of cementitious material and promotes more responsible utilization of steel industry by-products [29].

Among the available SCMs, GGBFS has been the subject of numerous studies evaluating its influence on the fresh and hardened properties of concrete, showing that higher replacement rates can lower production costs and enhance environmental sustainability [30, 31]. Ground granulated blast furnace slag (GGBFS) is an industrial by-product from the steel manufacturing process with great potential as a partial substitute for Portland cement [32, 33]. Ground granulated blast furnace slag (GGBFS) is an industrial by-product from the steel manufacturing process with high potential as a partial substitute for Portland cement [34]. In fact, since the early 20th century, slag-based cements have been used in Europe and North America in demanding structural applications [35, 36].

GGBFS is a vitreous, granular material obtained by rapid water cooling of molten slag from the blast furnace, primarily composed of calcium silicates and calcium aluminosilicates formed at temperatures around 1,500 °C [37, 38]. This granulated slag exhibits both cementitious and pozzolanic activity, which—once properly activated—promotes the formation of calcium silicate hydrate (C–S–H) gel, a key component in the strength development of hardened concrete [39]. Due to its latent hydraulic activity and pozzolanic reactivity, its incorporation into cement contributes to the progressive increase of long-term strength and material durability [40-42]. Moreover, its use favorably modifies various fresh and hardened-state properties by improving workability, reducing bleeding and heat of hydration, enhancing long-term strength and durability, and decreasing porosity and permeability [43-45].

GGBFS possesses cementitious and pozzolanic characteristics that make it a promising material for the partial replacement of ordinary Portland cement in both concrete and mortar formulations [46, 47]. Numerous studies have assessed its impact on the mechanical performance and durability of concrete, highlighting environmental advantages such as CO_2 reduction resulting from lower cement consumption [48]. Additionally, replacing a portion of cement with GGBFS reduces the emission of harmful gases and the energy demand during concrete production [49], achieving up to a 47.5% reduction in total greenhouse gas emissions compared to conventional concrete [50]. The incorporation of industrial by-products such as GGBFS and fly ash is considered a key strategy for mitigating climate change [51-53], as it not only enhances the valorization of waste materials but also offers both environmental and economic benefits [54]. Furthermore, GGBFS only requires grinding for use as a mineral addition, representing significant energy savings compared to clinker calcination [55].

GGBFS is recognized as one of the most beneficial SCMs for producing sustainable, high-quality concrete and is commonly used to reduce the proportion of Portland cement in mortars and concretes. Numerous studies have demonstrated that its incorporation significantly improves both fresh and hardened properties of the material, depending on the replacement ratio [56]. Its use enhances workability, densification, and durability, increases compressive and tensile strength, and reduces permeability and drying shrinkage [57-61]. For instance, compressive strength can increase by up to 20% when 30% of the cement is replaced by GGBFS, although this trend tends to decline when the replacement exceeds 40%, as observed with splitting tensile strength as well [62, 63]. In general, studies have confirmed that the optimal replacement proportion significantly enhances compressive strength, elastic modulus, and flexural strength [64-66], although these effects strongly depend on the fineness and reactivity of the GGBFS [67].

From a microstructural perspective, the addition of GGBFS densifies the cementitious matrix and reduces overall porosity through the pozzolanic reaction between slag and the $Ca(OH)_2$ released during cement hydration, promoting the formation of C–S–H gel [68,69]. Due to its lower density, GGBFS may slightly decrease the overall density of concrete; however, at later ages (e.g., 90 days), GGBFS-containing mixtures exhibit significant improvements in strength and workability, in compliance with EFNARC guidelines [70]. Furthermore, studies have concluded that using GGBFS as a partial replacement for Portland cement enhances both fresh and hardened concrete performance, contributing to reduced porosity and increased durability [71-73]. The fineness of GGBFS is a key factor governing its reactivity and its influence on the final microstructure [74].

In experimental studies where GGBFS was used as a binder and partial replacement for cement in proportions ranging from 2.5% to 12.5%, the highest compressive, flexural, and splitting tensile strengths were obtained with a 10% GGBFS substitution, demonstrating its potential for sustainable concrete production [75]. Additionally, research using

water-activated ground slag reported compressive strength increases of up to 166% at 28 days with only 2.5% replacement [76]. Factorial studies evaluating water-to-cement ratios (0.45 and 0.50) and GGBFS contents between 0% and 60% concluded that higher slag percentages improve strength and durability (greater density, lower absorption, and porosity), although higher water-to-cement ratios tend to reduce these properties; the interaction between both factors was not statistically significant [77-79].

Concrete workability decreases as GGBFS content increases, due to its high fineness and reactivity; thus, the use of superplasticizers is recommended when substitution exceeds 40% [80]. Moreover, a 30% replacement has been identified as optimal for balancing physical and mechanical properties, achieving slump values up to 30% higher than those of plain concrete while also reducing the cost of sustainable concrete production [81]. Consequently, studies conclude that replacing 30% to 40% of cement with GGBFS reduces overall costs while maintaining adequate workability and mechanical performance [80, 81].

In terms of mechanical performance, the use of GGBFS has been shown to positively influence compressive strength and long-term durability, primarily due to the secondary formation of C–S–H gel, which results in a denser structure less susceptible to environmental degradation [82]. However, it is essential to determine an appropriate GGBFS replacement ratio to avoid adverse effects, such as early-age cracking that may occur when excessively high contents are used [83, 84]. Nonetheless, some studies report favorable outcomes even under extreme conditions, such as replacing 40% of cement in recycled aggregate concrete (RAC) exposed to high temperatures [85].

It is estimated that in 2017, global GGBFS generation reached approximately 530 million tonnes, yet only 65% was utilized by the construction industry, highlighting its potential as an underutilized resource [53]. GGBFS has also been proposed as a precursor for geopolymer concrete, standing out for its environmental and technical advantages compared to traditional cement [86]. Accordingly, many cement-reduction strategies have prioritized the use of SCMs such as GGBFS and fly ash, based on their availability and durability-related performance [87]. These materials are incorporated into concrete either as components of blended cements or as additions to the fresh mix [88–90]. Moreover, the incorporation of GGBFS not only valorizes an industrial by-product, but also enhances various hardened-state properties and reduces drying shrinkage [91–93]. Therefore, its use in concrete and mortar represents a promising strategy to align environmental sustainability with mechanical performance, contributing to emissions reduction and more responsible consumption of natural resources.

Despite the extensive body of research on the use of GGBFS in concrete, significant gaps remain in the literature, particularly regarding the influence of different replacement ratios on the mechanical and microstructural properties of the material at both early and later ages under controlled experimental conditions. This study addresses this gap through a quantitative evaluation of the effect of partial cement replacement with GGBFS in concrete with a characteristic compressive strength of f'c = 280 kg/cm², analyzing its properties, their evolution over time, and their correlation with microstructural transformations. This approach aims to generate robust technical evidence to guide more sustainable construction decisions and to support the effective implementation of GGBFS in the structural concrete industry.

The results will contribute to establishing technical guidelines for the optimized use of GGBFS in structural applications, promoting a more sustainable and resilient construction model aligned with the principles of the circular economy.

2. Material and Methods

This study is framed within the domain of quantitative and applied research. Methodologically, it is classified as explanatory, as it seeks to analyze and elucidate the effects of partial replacement of Portland cement with ground granulated blast furnace slag (GGBFS) on the mechanical performance and microstructural development of concrete designed for a compressive strength (f'c) of 280 kg/cm².

The methodology employed a direct observation approach, allowing for systematic monitoring and detailed documentation of specimen behavior throughout the experimental process. Data collection was guided by a structured Observation Guide, specifically designed with objective criteria to ensure precision and consistency in capturing relevant information.

The study population comprised 140 concrete specimens, including cylindrical samples and prismatic beams, all produced with a design compressive strength of f'c = 280 kg/cm² and incorporating varying proportions of ground granulated blast furnace slag (GGBFS) as a partial replacement of Portland cement by weight. The aggregates used were sourced from quarries located in the Ica region, Peru. The specimens were categorized into five groups according to GGBFS content: 0.00% (control mix), 8.0%, 12.0%, 16.0%, and 20.0%. Curing was performed at 7, 14, and 28 days to assess the evolution of mechanical and microstructural properties over time.

Figure 1 presents a schematic diagram of the experimental procedure, outlining the key stages of the research methodology, including material preparation, specimen mixing and curing, and the mechanical and microstructural characterization techniques implemented.

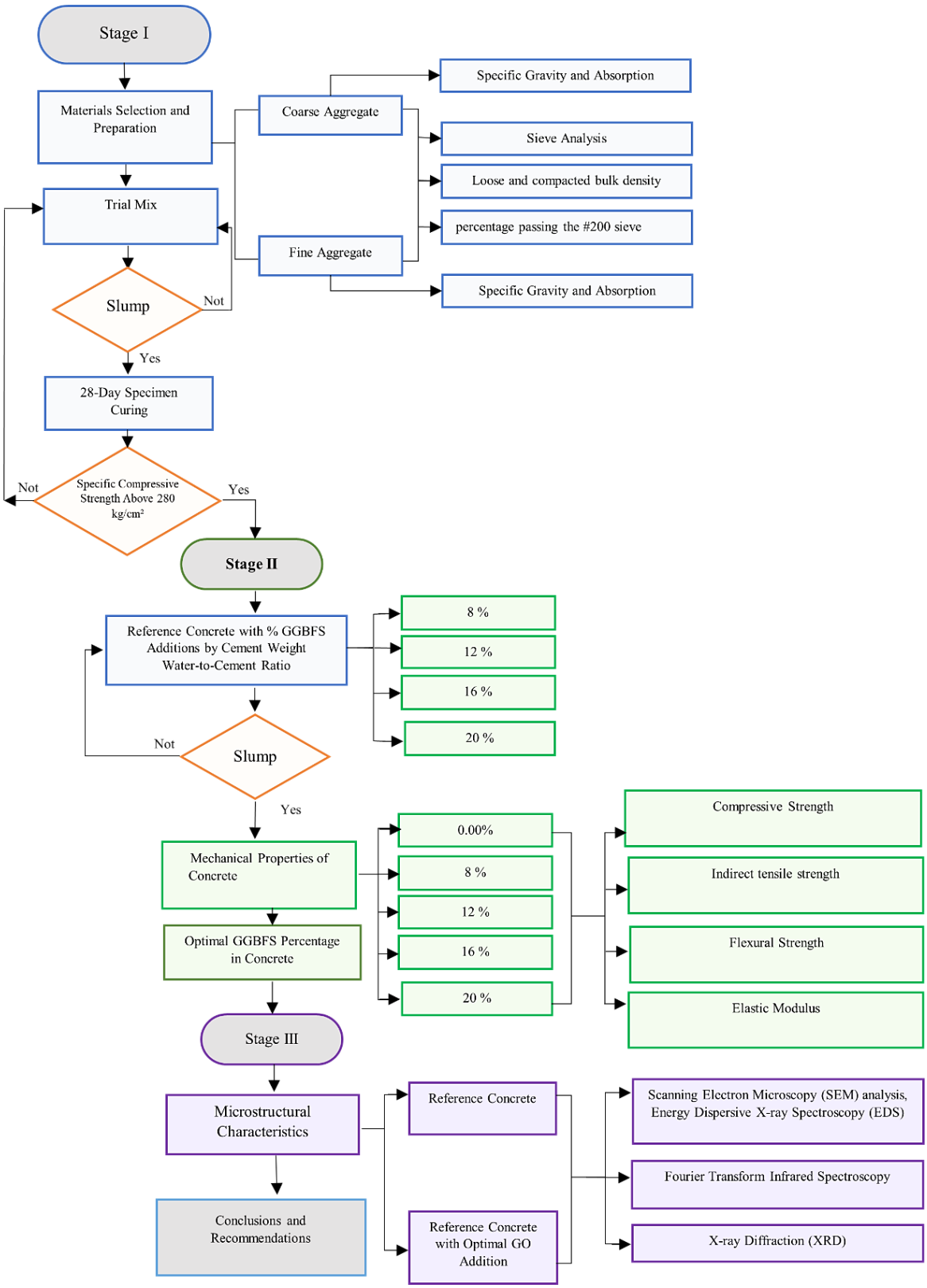

Figure 1. Schematic diagram of the experimental methodology

2.1. Characterization of Ground Granulated Blast Furnace Slag: Density, Blaine Specific Surface Area, and Chemical Composition

The ground granulated blast furnace slag (GGBFS) utilized in this study was supplied by Quanzhou Winnitoor Industry Co., Ltd. (Fujian, China), a recognized manufacturer specializing in by-products of the steel industry. According to the material's technical data sheet, the GGBFS is characterized by its specific gravity, bulk density, Blaine fineness, and chemical composition. Table 1 presents a comparative summary of these properties in relation to those reported in prior studies, providing a contextual basis for evaluating the material's characteristics within the broader research landscape.

Table 1. Physical and Chemical Characterization of Granulated Blast Furnace Slag (GGBFS)

Researchers	Physical Properties		Chemical Properties						
	Density (g/cm³)	Blaine Specific Surface (m²/kg)	% Calcium Oxide	% Silicon Dioxide	% Aluminium Oxide	% Magnesium Oxide	% Titanium Oxide	% Sodium Oxide	% Manganese Oxide
This study	2.90	434	44.00	36.60	11.80	5.70	0.50	0.50	0.20
López-Perales et al. [2]	2.61	-	37.71	35.56	10.87	7.12	2.28	0.68	2.61
Abdellatief et al. [66]	2.88	400	45.88	30.38	9.05	5.39	-	0.52	-
Sara et al. [94]	2.82	380	42.20	40.00	6.00	4.70	1.20	-	-
Mehta et al. [95]	2.68	485	35.68	35.80	13.21	9.76	-	0.48	-
Kim et al. [68]	2.91	405	42.20	40.00	6.00	4.70	1.20	-	-
Tang et al. [65]	2.91	-	42.60	38.00	13.80	8.50	-	0.21	0.40
Ustabasi & Kaya [74]	-	466.6	35.30	38.10	11.40	7.92	0.44	0.29	-

2.2. Aggregates, Cement, and Supplementary Material

Laboratory tests were carried out to assess the mechanical and microstructural behavior of the reference concrete (f'c = 280 kg/cm²), serving as a baseline for comparison with GGBFS-modified mixes

The aggregates used in this study were sourced from the Palomino-Parcona quarry, located in the Ica region (Table 2). The particle size distribution of the aggregates was determined in accordance with ASTM C136/C136M-19 [96]. The gradation curves for the fine and coarse aggregates are presented in Figures 2-a and 2-b, respectively. Sol Type I cement was used for concrete production.

Table 2. Evaluation of the Degradation Resistance of Coarse Aggregates Sourced from the Palomino–Parcona Quarry

Aggregate Source	Maximum Nominal Size	Aggregate Gradation	Initial Mass	Mass Retained on Sieve No. 12	Percentage of Wear (Passing Sieve No. 12)
Palomino-Parcona	1/2"	B	5000	4326	13.48%

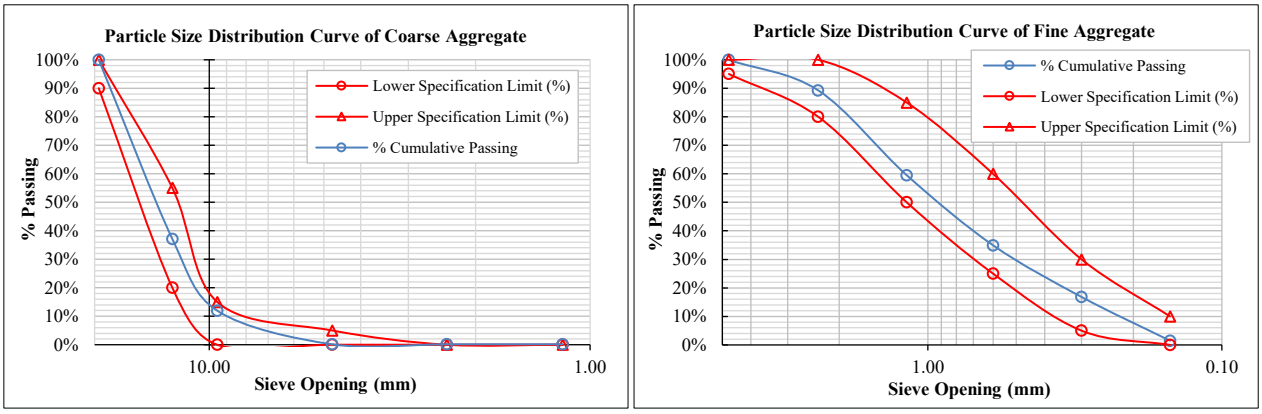

(a) (b)

Figure 2. Particle size distribution curves of the aggregates: (a) fine aggregate; (b) coarse aggregate

In accordance with the ACI 211.1-91 (Reapproved 2009) [97] method adopted in this study; the mix design parameters listed in Table 3 were kept constant to ensure consistent reference conditions across all experimental mixtures.

Table 3. Constant mix design parameters according to ACI 211.1-91

Parameter	Value / Description
Mix design method	5, 10, 15, 20
Water-to-cement ratio (w/c)	0.466 (constant for all mixtures)
Aggregate source	Palomino Quarry (Ica, Peru); consistent physical properties
Base mix proportions (per kg of cement)	Fine aggregate (F.A.): 1.86 kg
	Coarse aggregate (C.A.): 1.68 kg
	Water: 19.51 L
Type of cement	ASTM C150-compliant Type I Portland cement (Sol brand)
Curing method	Water immersion at ambient temperature, according to ASTM C192/C192M-19 [98]

Maintaining these parameters constant ensures the validity of the comparative analysis, as the only variable among the mixtures is the level of GGBFS replacement (0%, 8%, 12%, 16%, and 20%). This controlled approach allows for the observed differences in mechanical properties to be specifically attributed to the influence of GGBFS, thereby isolating its effect within the experimental framework and minimizing potential confounding factors.

In addition, concrete mixtures were prepared incorporating ground granulated blast furnace slag (GGBFS) at replacement levels of 8.0%, 12.0%, 16.0%, and 20.0% by weight of cement. The selection of GGBFS dosages—0.00%, 8.0%, 12.0%, 16.0%, and 20.0%—was informed by an extensive review of prior studies, which report notable variations in compressive strength within this range. Optimal performance is commonly observed between 10% and 20%, depending on the characteristics of the cementitious matrix, as summarized in Table 4. The 0.00% GGBFS content corresponds to the control mix (without supplementary material), whereas the progressive incorporation of GGBFS enables a systematic evaluation of mechanical performance trends and the identification of potentially optimal replacement levels. This experimental design also facilitates comparison with existing literature, thereby strengthening the interpretative framework for analyzing the results within a broader scientific context.

Table 4. Optimal replacement levels of ground granulated blast furnace slag (GGBFS) for enhancing compressive strength, as reported in previous studies

Researchers	GGBFS Percentage (%)	Optimal GGBFS Percentage (%)	Compressive Strength Improvement (%)
Bheel et al. [99]	5, 10, 15, 20	10	+12,28
Qi et al. [100]	10, 20, 30, 40, 50	20	-2.4
Shen et al. [83]	20, 35, 50,	20	-10.0
Tung et al. [21]	5, 10	5	12.59

Mechanical testing was carried out under controlled laboratory conditions in accordance with the corresponding ASTM standards, using standardized specimens distributed across different curing ages to evaluate the performance of concrete incorporating ground granulated blast furnace slag (GGBFS).

Compressive strength (Figure 3-a) was determined using 50 cylindrical specimens (10 cm × 20 cm), arranged in sets of three tested at 7 days, three at 14 days, and four at 28 days for both the control mix and each GGBFS replacement level, following the procedures outlined in ASTM C39/C39M-18 [101].

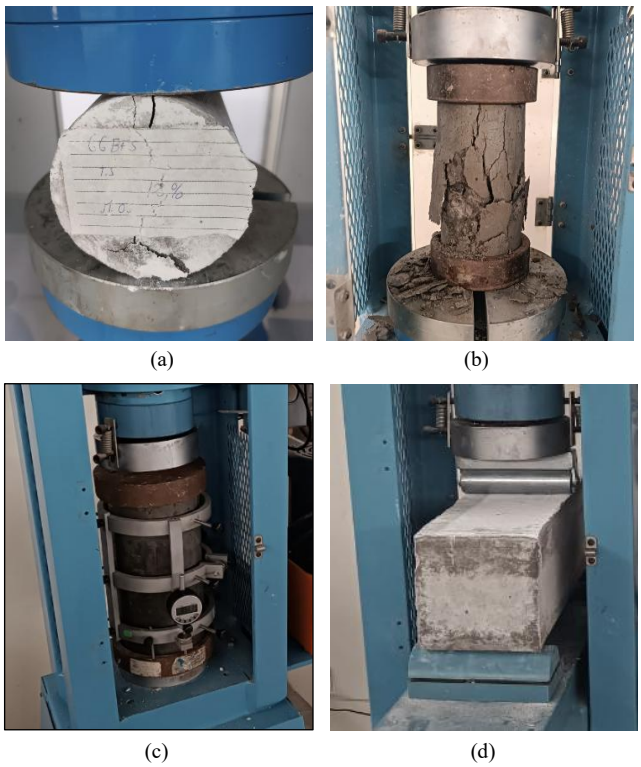

(a) (b) (c) (d)

Figure 3. Mechanical tests on reference concrete and modified concrete with additions of 8%, 12%, 16%, and 20% GGBFS: (a) Compressive strength test of cylindrical concrete specimens ($f'c$); (b) Splitting Tensile Strength of Cylindrical Concrete Specimens (f_t); (c) Flexural Strength of Concrete (Using Simple Beam with Center-Point Loading) (f_r); (d) Static Modulus of Elasticity Test for Concrete in Compression (E_c).

Splitting tensile strength (Figure 3-b) was assessed using 35 cylindrical specimens (10 × 20 cm), with three specimens tested at 7 days and four at 28 days for each mix, according to ASTM C496/C496M-17 [102].

Flexural strength (Figure 3c) was evaluated using 35 prismatic beams (15 × 15 × 51 cm), with three specimens tested at 7 days and four at 28 days for each GGBFS content, in accordance with ASTM C293/C293M-16 [103].

Lastly, the static modulus of elasticity (Figure 3d) was determined from 20 cylindrical specimens (10 × 30 cm), with four specimens tested at 28 days for the reference mix and each GGBFS percentage, following ASTM C469 / C469M-22 [104].

Table 5 details the mix design, including the water-to-cement ratio (W/C), as well as the specific proportions of GGBFS, aggregates, cement, and water used in the study.

Table 5. Aggregate quantities used for mechanical strength and modulus of elasticity tests in control and GGBFS-modified concrete mixtures (8%, 12%, 16%, and 20%)

Substitution level (%)	Cement (kg)	Fine Agg. (kg)	Coarse Agg. (kg)	Water (L)	Replacement GGBFS
+ 0 %	1	1.86	1.68	19.51	0.00
+ 8 %	0.92	1.86	1.68	19.51	0.08
+ 12 %	0.88	1.86	1.68	19.51	0.12
+ 16 %	0.84	1.86	1.68	19.51	0.16
+ 20 %	0.80	1.86	1.68	19.51	0.20

The effect of GGBFS incorporation on the workability of concrete was evaluated through the slump test, in accordance with ASTM C143/C143M. The results, summarized in Table 6, show variations in mixture consistency depending on the percentage of cement replacement by GGBFS. At low replacement levels (8% and 12%), a reduction in slump was observed, indicating decreased workability. In contrast, higher substitution levels—particularly at 20%—resulted in increased slump values, reaching up to 10.41 cm, suggesting improved mixture fluidity. This enhancement may be attributed to a lubricating effect produced by the fine slag particles. These findings demonstrate that the influence of GGBFS on workability is non-linear and is governed by both its dosage and its physical interaction with the cementitious matrix.

Table 6. Effect of GGBFS content on concrete slump

GGBFS Content (%)	Slump (in)	Slump (cm)
0 %	3.80″	9.65 cm
8 %	2.70″	6.86 cm
12 %	2.40″	6.10 cm
16 %	3.40″	8.64 cm
20 %	4.10″	10.41 cm

It was observed that intermediate GGBFS replacement levels (8% and 12%) led to a reduction in workability compared to the control mix, while a 20% replacement resulted in improved workability, surpassing even the reference mixture. This suggests that, beyond a certain threshold, the presence of fine slag particles may enhance mixture fluidity through a lubricating effect. However, a limitation of this study is that setting times were not evaluated, which may be relevant given the known influence of GGBFS on the hydration kinetics of blended cements.

Following the identification of the optimal GGBFS replacement percentage, hardened concrete specimens were extracted for the microstructural characterization of both the reference mix and the mix incorporating the optimal GGBFS content, enabling a comparative analysis between the two.

3. Results

3.1. Mechanical Properties of Concrete: Compressive Strength, Indirect Tensile Strength, Flexural Strength, and Modulus of Elasticity

f′c: Compressive Strength of Concrete

Table 7 summarizes the compressive strength results of concrete specimens incorporating varying proportions of ground granulated blast furnace slag (GGBFS) at curing ages of 7, 14, and 28 days. The results indicate that the partial replacement of cement with GGBFS leads to an enhancement in compressive strength compared to the control mix

(0.00%). The highest strength was recorded at a replacement level of 20%, exhibiting a consistent and marked increase across all curing periods. Intermediate replacement levels of 8% and 12% also demonstrated strength improvements relative to the control; however, these values remained below those obtained with 16% and 20% GGBFS. Figure 4 supports these findings by illustrating the evolution of compressive strength over curing time, indicating that the beneficial effects of GGBFS become more pronounced at later ages and higher replacement levels. These results underscore the importance of properly controlling the amount of GGBFS incorporated in the mix in order to optimize the mechanical performance of the concrete.

Table 7. Comparison of concrete compressive strength results (f′c) in kg/cm²

Ground Granulated Blast Furnace Slag Addition by Cement Weight (%)	Curing Age		
	7 Days	14 Days	28 Days
0.00% (reference concrete)	279.12	326.46	348.17
8%	263.92	295.51	391.54
12%	266.75	302.84	375.64
16%	300.42	345.96	400.43
20%	298.53	336.91	408.58

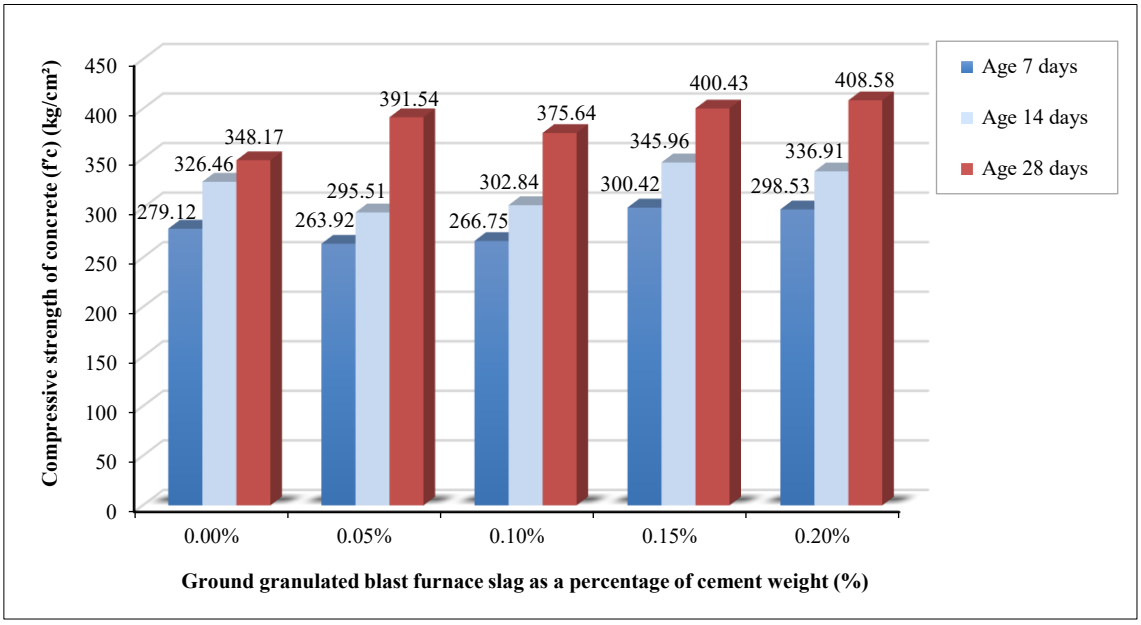

Figure 4. Comparison of concrete compressive strength results (f′c) in kg/cm²

The study monitored the development of compressive strength at 7, 14, and 28 days—key ages for assessing the performance of supplementary cementitious materials such as ground granulated blast furnace slag (GGBFS), whose pozzolanic activity primarily manifests at medium and later ages. The results revealed variability in compressive strength at 7 days compared to the control mixture, whereas at 28 days, the mixture with 20% cement replacement by GGBFS exhibited the best performance, with a 6.35% increase in compressive strength. This evaluation methodology is appropriate given that GGBFS requires a slower activation process to form cementitious products through secondary pozzolanic reactions.

f_t: Indirect Tensile Strength of Concrete

Table 8 presents the average indirect tensile strength results (in kg/cm²) of concrete mixes incorporating different percentages of Ground Granulated Blast Furnace Slag (GGBFS) as an additive, evaluated at 7 and 28 days of curing. It is observed that the control mix (0% GGBFS) exhibits the highest strength at 7 days (27.59 kg/cm²). At 28 days, the tensile strength shows a slight reduction with GGBFS incorporation up to 12%, followed by a recovery to values close to the control mix when the GGBFS content reaches 20%. Figure 5 further reinforces this trend, highlighting that although early-age strength (7 days) decreases with GGBFS inclusion, a progressive recovery is observed at 28 days. This behavior suggests a positive contribution of GGBFS to long-term mechanical performance, likely attributed to its latent pozzolanic activity.

Table 8. Comparison of concrete indirect tensile strength results (ft) in kg/cm²

Ground Granulated Blast Furnace Slag Addition by Cement Weight (%)	Curing Age	
	7 Days	28 Days
0.00% (reference concrete)	27.59	29.67
8%	16.35	27.38
12%	21.68	24.03
16%	23.62	25.31
20%	23.39	27.84

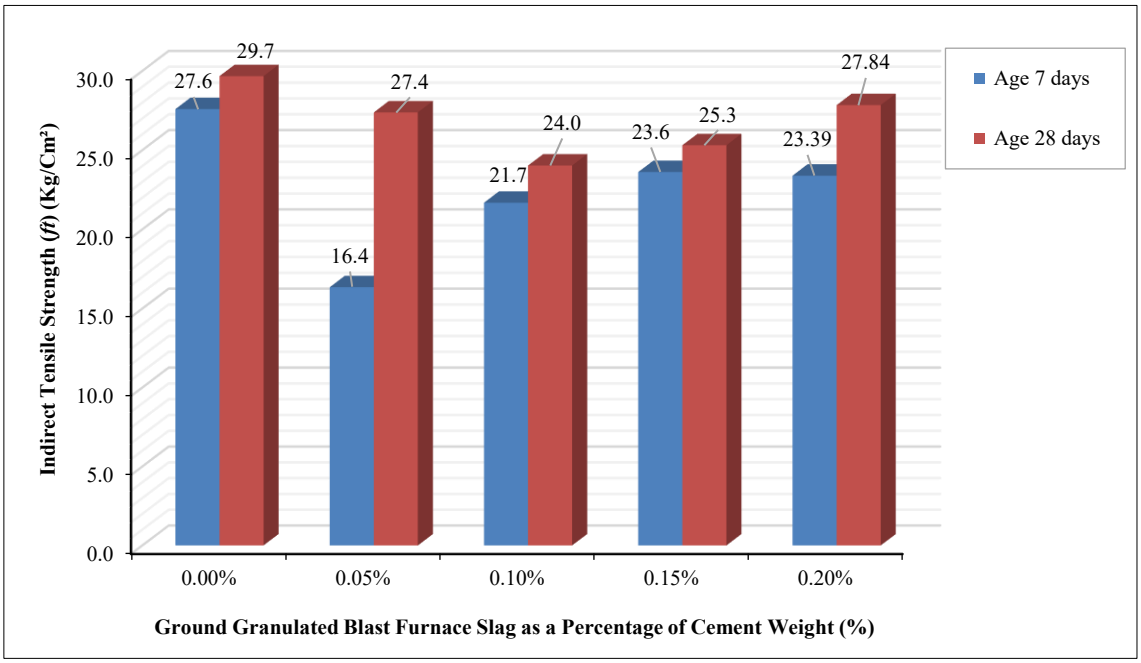

Figure 5. Comparison of concrete indirect tensile strength results (ft) in kg/cm²

f_r: Flexural Strength of Concrete

Table 9 presents the average flexural strength results (in kg/cm²) of concrete mixes incorporating various percentages of Ground Granulated Blast Furnace Slag (GGBFS), evaluated at 7 and 28 days of curing. The data indicate that the incorporation of GGBFS enhances early-age flexural strength, with the 20% replacement yielding the highest value at 7 days (47.94 kg/cm²), surpassing the control mix (41.35 kg/cm²). At 28 days, the mix with 8% GGBFS exhibits the maximum strength (73.48 kg/cm²), whereas higher replacement levels tend to result in a slight reduction. Figure 6 illustrates this behavior, showing a consistent improvement in early-age flexural strength with increasing GGBFS content, while long-term strength peaks at moderate GGBFS levels and stabilizes thereafter. These results suggest that partial substitution with GGBFS can enhance flexural performance, particularly at early ages, likely due to microstructural densification and the pozzolanic reactivity of the slag.

Table 9. Comparison of concrete flexural strength results (f_r) in kg/cm²

Ground Granulated Blast Furnace Slag Addition by Cement Weight (%)	Curing Age	
	7 Days	28 Days
0.00% (reference concrete)	41.35	61.8
8%	43.12	73.48
12%	45.83	59.50
16%	45.16	60.08
20%	47.94	60.27

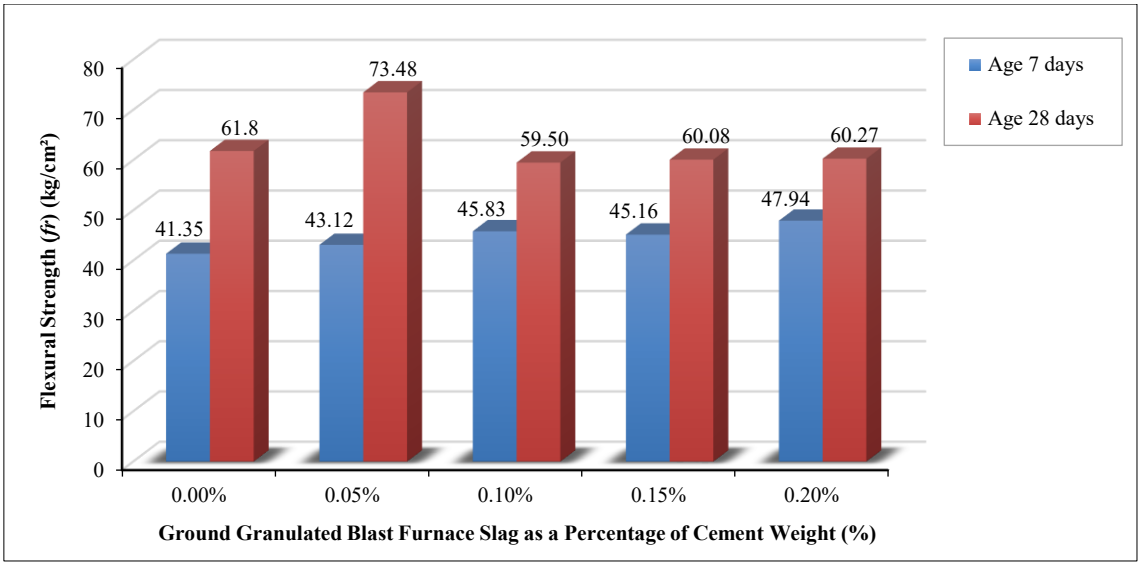

Figure 6. Comparison of concrete flexural strength results (f_r) in kg/cm²

E_c: Modulus of Elasticity

Table 10 shows the average modulus of elasticity (in kg/cm²) at 28 days for concrete mixes incorporating various percentages of Ground Granulated Blast Furnace Slag (GGBFS). The results reveal a general improvement in stiffness with the inclusion of GGBFS compared to the control mix (290,225.45 kg/cm²). The maximum modulus is observed at 20% GGBFS replacement, reaching 304,662.46 kg/cm². Although a slight decrease is noted at 12% substitution (287,045.45 kg/cm²), values at 8% and 16% also demonstrate significant enhancement (300,796.71 and 300,308.60 kg/cm², respectively). Figure 7 visually reinforces this trend, indicating that GGBFS contributes positively to the elastic behavior of concrete at 28 days, likely due to the improved packing density and pozzolanic activity of the slag, which refines the microstructure and increases the material's stiffness.

Table 10. Comparison of concrete modulus of elasticity results (E_c) at 28 days (kg/cm²)

Ground Granulated Blast Furnace Slag Addition by Cement Weight (%)	Curing Age
	28 Days
0.00% (reference concrete)	290225.45
8%	300796.71
12%	287045.45
16%	300308.60
20%	304662.46

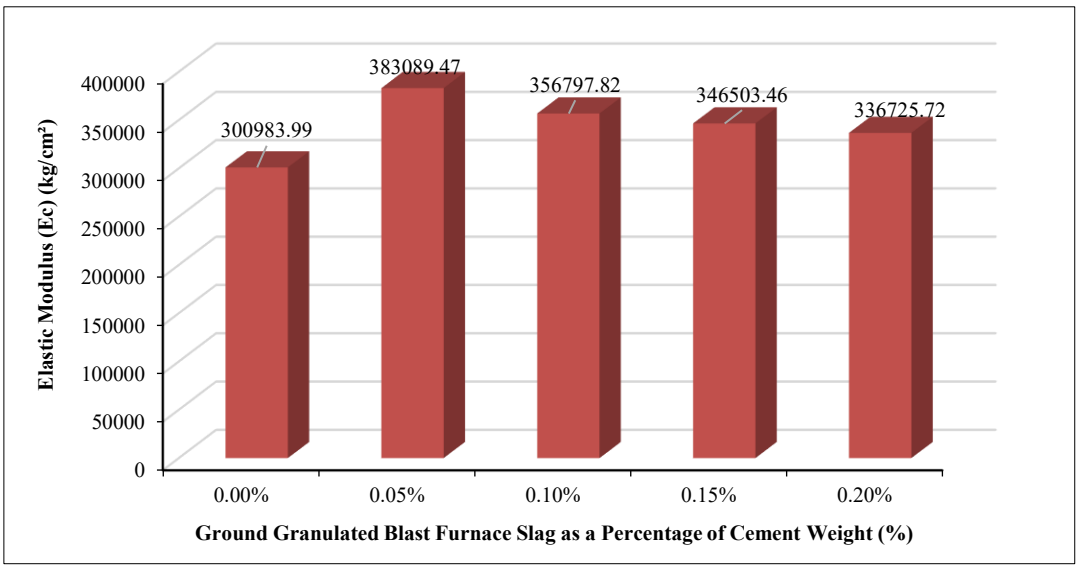

Figure 7. Comparison of concrete modulus of elasticity results (E_c) at 28 days (kg/cm²)

The mechanical test results presented in this study are supported by a robust statistical framework that reinforces the reliability and reproducibility of the findings. Normality of the data was verified using the Shapiro–Wilk test ($p > 0.05$ for all properties), and homogeneity of variances was confirmed through Levene's test ($p > 0.05$). Analysis of variance (ANOVA) was employed to detect statistically significant differences among groups, complemented by the Tukey HSD test for multiple comparisons. Additionally, the Kruskal–Wallis test was used as a non-parametric validation tool. Reproducibility was ensured by testing 3 to 4 specimens per age and property, with all results exhibiting acceptable coefficients of variation. Notably, significant differences were observed only in the elastic modulus ($p = 6.9 \times 10^{-4}$), highlighting its sensitivity to GGBFS incorporation relative to other mechanical properties.

Statistical Evaluation of Mechanical Properties at 28 Days for GGBFS-Modified Concrete Mixtures

At 28 days of curing, the mechanical properties of the specimens were evaluated through compressive strength, tensile strength, flexural strength, and modulus of elasticity tests. Based on the obtained results, a statistical assessment was conducted to determine whether the experimental mixtures incorporating varying percentages of GGBFS exhibited significant differences compared to the control concrete. The aim was to identify the optimal replacement percentage of GGBFS. Prior to the comparative analysis, two preliminary statistical tests were performed: a normality test and a homoscedasticity test (equality of variances among groups). These tests were essential to determine the appropriate statistical approach—parametric or non-parametric—for the subsequent analysis.

Shapiro–Wilk and Levene's tests yielded p-values ranging from 0.112 to 0.476 across the four mechanical properties, supporting the assumptions of normality and homoscedasticity required for parametric analysis. Therefore, one-way ANOVA was applied, complemented by the Kruskal–Wallis test as a confirmatory non-parametric method. One-way ANOVA indicated no significant differences in compressive strength ($F(4,15)=1.35$, $p=0.230$) or indirect tensile strength ($F(4,15)=2.52$, $p=0.080$), whereas significant effects were detected for flexural strength ($F(4,15)=7.84$, $p=0.0013$) and elastic modulus ($F(4,15)=9.01$, $p=6.9\times10^{-4}$). These findings were corroborated by Kruskal–Wallis ($\chi^2(4)=4.50$, $p=0.3425$; $\chi^2(4)=7.92$, $p=0.0945$; $\chi^2(4)=9.99$, $p=0.0407$; $\chi^2(4)=14.11$, $p=0.0069$, respectively).

Post-hoc Tukey HSD analysis revealed that, in flexural strength, the control mix differed significantly from the 8 % GGBFS blend ($p=0.0102$), which in turn differed from higher replacement levels ($p<0.005$). For elastic modulus, only the 20 % GGBFS substitution exhibited a significant increase relative to the control ($p=0.0082$).

3.2. Microstructural Characteristics of the Reference Concrete Sample and the Sample with 20% Ground Granulated Blast Furnace Slag

FTIR: Absorbance in Fourier Transform Infrared Spectroscopy

The absorbance units and corresponding absorption bands were characterized using Fourier Transform Infrared Spectroscopy (FTIR), in accordance with the ASTM E1252-98(2021) [105]. This methodology facilitated the identification of chemical functional groups associated with the absorbance peaks in both the control concrete sample and the modified concrete sample incorporating 20% GGBFS. The analysis was performed using a Bruker Tensor 27 FTIR spectrometer, equipped with a diamond attenuated total reflectance (ATR) accessory (Bruker, Ettlingen, Germany).

In this context, the FTIR spectra of the reference sample and the sample with 20% GGBFS are presented, allowing for the analysis of their molecular composition. In Figure 8-a, the reference concrete exhibits characteristic absorbance peaks at 965 cm^{-1}, 874 cm^{-1}, and 1412 cm^{-1}, with corresponding intensities of 0.08925, 0.05898, and 0.02271 units. These peaks are associated with the vibrational modes of Si–O and C–O (carbonates) bonds, as well as other functional groups present in the cementitious matrix. In Figure 8-b, which corresponds to the sample with 20% cement replacement by GGBFS, slight shifts in peak positions are observed at 968 cm^{-1}, 875 cm^{-1}, and 1415 cm^{-1}, accompanied by increased intensities of 0.12515, 0.08425, and 0.03564 units, respectively. These shifts suggest improved molecular interaction and the integration of slag-derived functional groups. The observed spectral variations suggest improved chemical reactivity, particularly in the formation of C–S–H and C–A–S–H phases associated with cement hydration. Furthermore, the increased absorbance in the 800–1000 cm^{-1} region suggests a denser cementitious matrix, without altering the primary chemical structure of the system. Figure 8-c compares both spectral curves, confirming a general increase in absorbance for the GGBFS-modified sample. This supports the hypothesis that partial cement replacement with GGBFS promotes greater formation of hydration products, improves concrete microstructure, and enhances the chemical stability of the cementitious system.

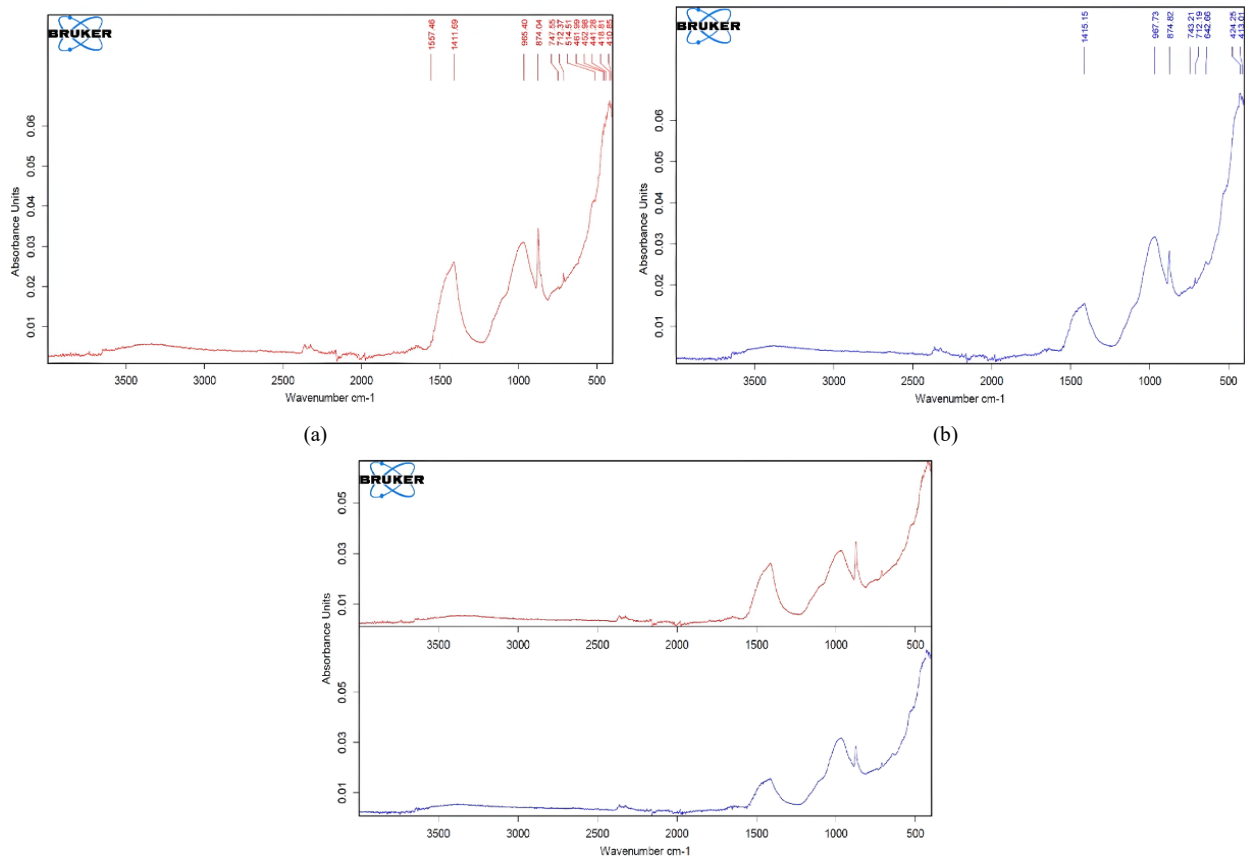

Figure 8. Absorbance units and absorption bands: (a) FTIR spectrum of the reference sample; (b) FTIR spectrum of the reference sample with 20% GGBFS; (c) comparison of the FTIR spectra of the reference sample and the sample with 20% GGBFS.

Chemical Composition of Concrete Samples by Scanning Electron Microscopy (SEM) and Energy-Dispersive X-Ray Spectroscopy (EDS)

For sample preparation, fragments with the appropriate geometry were selected to represent both the reference concrete (Figure 9-a) and the modified concrete incorporating 20% GGBFS (Figure 9-b). Regarding sample preparation, a representative portion of each concrete was selected and individually mounted on the scanning electron microscope (SEM) sample holder. Measurements were performed under low vacuum conditions with water vapor injection to prevent the accumulation of surface charge on the samples and to allow analysis without gold coating. This approach was implemented to avoid biases in the EDS measurements.

Figure 9. Morphological and compositional analysis: (a) representative sample of reference concrete; (b) representative sample of modified concrete incorporating 20% GGBFS

Compositional analysis of the concrete samples was conducted using scanning electron microscopy (SEM) coupled with energy-dispersive X-ray spectroscopy (EDS), following the guidelines of ASTM C1723-16(2021) [106]. The analyses were performed with a FEI Quanta 200 SEM (FEI Company, Hillsboro, OR, USA), operating at an accelerating voltage of 30 kV and a spot size of 6, enabling both high-resolution imaging and elemental characterization. Selected areas of interest were examined at magnifications ranging from 45× to 50× EDS analysis was carried out using an EDAX

detector (EDAX, Ametek Materials Analysis Division, Mahwah, NJ, USA) integrated into the SEM system. Elemental data were processed using the EDAX Genesis XM 4 software, with compositional quantification based on ZAF matrix correction protocols.

Figures 10-a and 10-b show SEM micrographs of the reference concrete sample at low magnification (50×), acquired with an LFD detector at 30 kV and a working distance of approximately 15 mm, revealing smooth globular deposits (P1–P2) adjacent to porous, fissured matrix regions (P3–P4). In contrast, the micrographs of the concrete modified with 20 % GGBFS (Figures 10-c and 10-d), obtained under identical imaging conditions, exhibit a markedly irregular texture with fibrillar structures and pores of varying size. In all images, the marked points P1–P4 denote locations selected for point-specific compositional and topographical analyses, highlighting secondary-electron contrast between dense phases and more fragmented, heterogeneous regions. These images allow for a comparison of the distribution and chemical composition of the phases present in both samples, as detailed in Tables 11 and 12.

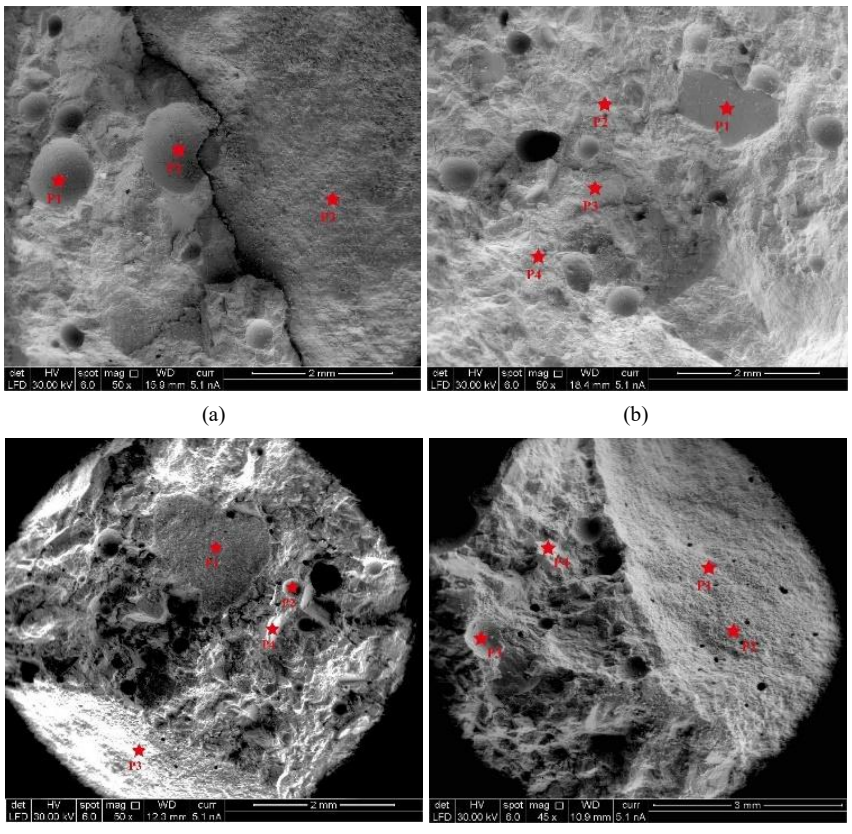

Figure 10. Morphological analysis and distribution of energy-dispersive spectroscopy (EDS) points in reference concrete and concrete modified with 20% GGBFS: (a) distribution of EDS analysis points (P1, P2, and P3) in the reference concrete sample; (b) distribution of EDS analysis points (P1, P2, P3 and P4) in the reference concrete sample; (c) distribution of EDS analysis points (P1, P2, P3, and P4) in concrete modified with 20% GGBFS; (d) distribution of EDS analysis points (P1, P2, P3, and P4) in concrete modified with 20% GGBFS.

Table 11. Chemical composition of the reference concrete sample

EDS Points		Atomic %									
		O	Na	Mg	Al	Si	S	K	Ca	Ti	Fe
Figure 9a	P3	70.23	1.05	0.66	1.99	4.74	0.39	0.38	19.68	-	0.88
	P4	76.61	1.16	0.84	2.31	5.75	-	0.37	12.13	-	0.84
	P1	63.11	-	0.44	1.55	4.76	0.52	0.63	28.01	-	0.97
Figure 9b	P1	66.66	-	6.14	6.50	13.84	-	3.82	1.62	0.88	6.54
	P2	74.24	-	-	2.39	7.29	-	0.43	14.10	-	1.55
	P3	59.02	-	5.31	5.17	11.28	-	3.07	6.12	1.26	8.79
	P4	68.57	-	-	1.15	4.20	-	0.22	24.58	-	1.29
Average		68.63	1.11	2.68	2.72	7.12	0.46	1.27	15.75	1.07	2.98

Table 12. Chemical composition of the reference concrete modified with 20% GGBFS

EDS Points		Atomic %									
		O	F	Na	Mg	Al	Si	S	K	Ca	Fe
Figure 9c	P1	66.99	-	0.67	0.19	1.70	5.26	0.21	0.35	29.88	0.76
	P2	65.84	-	0.78	0.35	1.64	5.21	0.34	0.22	24.78	0.84
	P3	66.82	-	0.74	0.20	1.64	5.48	0.40	0.27	23.48	0.95
	P4	72.37	2.04	1.58	0.85	2.14	5.18	0.23	0.33	14.54	0.73
Figure 9d	P1	74.03	-	-	1.03	3.32	-	-	21.62	-	-
	P2	74.88	-	-	1.88	6.85	-	-	16.40	-	-
	P3	70.93	-	1.19	2.14	6.37	-	-	18.28	-	1.10
	P4	67.08	3.28	-	6.78	16.58	-	3.21	3.07	-	-
Average		69.12	2.66	0.99	1.68	5.03	5.28	0.88	7.57	23.17	0.88

Based on the images obtained by secondary electrons, a notable morphological diversity in the concrete is evident. Fractured zones, which are characteristic of this type of mix, are identified alongside highly rounded grains, possibly indicative of the presence of belite; an essential component in the concrete formation process. Additionally, transition zones between the cement matrix and conventional aggregates are clearly observed, which is crucial for understanding the material's integrity and strength. The analysis of the cement matrix composition in both the concrete with 20% GGBFS and the reference concrete reveals a predominance of calcium (Ca) and oxygen (O). To a lesser extent, elements such as silicon (Si), sodium (Na), magnesium (Mg), aluminum (Al), potassium (K), and iron (Fe) are also detected. The similarity in the recorded values between the two samples suggests consistency in the formulation and processing of the concrete, despite the inclusion of GGBFS.

In the concrete with 20% GGBFS, the matrix presents values of up to 48.9 %wt Ca and 45.21 %wt O, whereas the reference concrete shows values of up to 46.5 %wt Ca and 55.85 %wt O. Regarding the conventional aggregates, they generally exhibit similar values for the predominant elements (Ca and O) as well as for the minor elements. However, differences are observed in the silicon (Si) content; the concrete with GGBFS shows slightly higher Si levels compared to the reference concrete, possibly because the GGBFS contains a higher silicon content than the conventional materials used in cement production. Additionally, in the reference concrete, certain grains with trace amounts of titanium (Ti) up to 2.46 %wt have been detected, which could indicate the presence of additives or impurities in the materials used during production.

3.2.3. Phase Chemical Composition Analysis by X-Ray Diffraction (XRD)

The identification of crystalline phases was carried out through X-ray diffraction (XRD) analysis, following the UNE-EN 13925-1:2006 standard [107]. The measurements were performed using a Panalytical AERIS diffractometer (Malvern Panalytical, Almelo, Netherlands), equipped with a cobalt (Co) anode and operating with a predefined Kα radiation wavelength. This setup enabled accurate determination of the phase composition of the concrete samples.

The results presented in Table 13 show that the incorporation of 20% GGBFS induces significant changes in the chemical and mineralogical composition of the concrete matrix. The most prominent variations include a substantial decrease in albite (from 47.5% to 24.8%) and amorphous content (from 38.0% to 21.8%), indicating that the addition of GGBFS promotes the formation of new crystalline phases through pozzolanic reactions. New crystalline phases—such as montebrasite (25.0%), $Bi_{10}Sr_{15}Fe_{10}O_{46}$ (24.8%), and $BaNiS_2$ (25.0%)—appear exclusively in the GGBFS-modified sample, reflecting a transformation of hydration products and increased mineralogical complexity. These newly formed compounds may contribute to improved chemical stability and durability of the hardened concrete. Moreover, the slight increase in calcite (+2.6%) and the emergence of phases such as polybasite and $Na_2Al_3(OH)_2(PO_4)_3$ suggest secondary reactions and the influence of GGBFS-derived constituents. The reduction or disappearance of some minor phases (e.g., $CuAlTe_2$) further indicates potential dilution or transformation effects within the matrix.

Table 13. Comparative phase composition of the reference concrete and the 20% GGBFS-modified concrete based on X-ray diffraction (XRD) analysis

Chemical Compounds	Unit	Reference Sample	Concrete modified with 20% GGBFS	Variation (%)
Mn Ni	%	-	0.40	+0.40
Calcite	%	11.30	13.90	+2.6
Bornite	%	-	0.10	+0.10
Albite	%	47.50	24.80	−22.7
Polybasite	%	-	1.00	+1.0
(Al0.5 Ga0.5) Co	%	-	0.10	+0.10
Bi_{10} Sr_{15} Fe_{10} O_{46}	%	0.80	24.80	+24.00
Ba Ni S_2	%	0.50	25.00	+24.50
(Cu Ti) Ni_2	%	0.80	0.30	−0.50
Na_2 Al_3 $(OH)_2$ $(PO_4)_3$	%	-	0.90	+0.90
4303494 (complex compound)	%	-	9.10	+9.10
Fettelite	%	-	0.40	+0.40
Montebrasite	%	-	25.00	+25.00
Cs Ag (Fe F_6)	%	-	2.20	+2.20
Potassium sulfate - $-beta	%	0.90	-	−0.90
Cu Al Te_2	%	0.20	-	−0.20
Amorfo	%	38.00	21.80	−16.20

These findings are further supported by the X-ray diffraction patterns shown in Figure 11, which illustrate the morphological differences between the reference concrete sample (Figure 11-a) and the concrete sample modified with 20% GGBFS (Figure 11-b). In the reference sample, dominant peaks correspond to albite, calcite, and minor quantities of $CuAlTe_2$ and $BaNiS_2$, indicating a relatively simple crystalline structure. In contrast, the GGBFS-modified sample exhibits a greater diversity of crystalline phases, with newly identified peaks corresponding to montebrasite, $Bi_{10}Sr_{15}Fe_{10}O_{46}$, polybasite, and fettelite, among others. The increased peak intensity and multiplicity in the modified sample confirm the enhanced formation of secondary reaction products, aligning with the compositional changes previously described in Table 11. This mineralogical evolution underscores the active role of GGBFS in refining the phase composition of the concrete matrix, potentially contributing to improved durability and microstructural stability. From a property standpoint, the formation of new crystalline phases contributes to matrix densification, which can enhance mechanical strength and resistance to aggressive agents. The observed increase in calcite content suggests a higher degree of carbonation, which may influence long-term durability through pore refinement and $CaCO_3$ precipitation. Additionally, the emergence of montebrasite is indicative of specific chemical pathways activated during the hydration process, further supporting the complex pozzolanic and latent hydraulic behavior of GGBFS within the blended system.

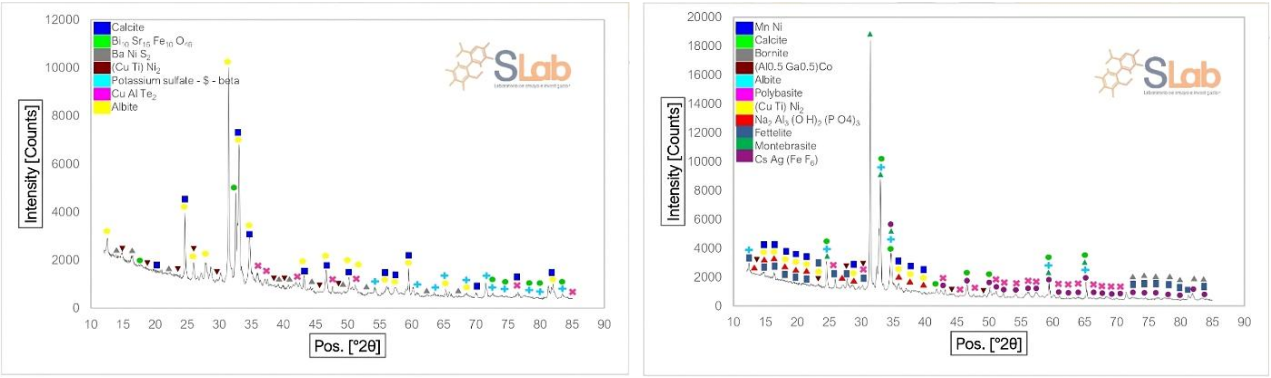

(a) (b)

Figure 11. Morphological X-Ray Diffraction Phase-Based Chemical Composition: (a) Diffractogram of the reference concrete sample and identified crystalline phases (b) Diffractogram of the reference concrete sample with 20% GGBFS and identified crystalline phases.

The newly identified crystalline phases have relevant implications for the long-term durability of the GGBFS-modified concrete matrix. The formation of stable mineral phases contributes positively to matrix densification, reducing overall porosity and permeability. Additionally, the observed decrease in portlandite ($Ca(OH)_2$) content suggests lower susceptibility to leaching and chemical degradation, while the development of chemically stable compounds enhances the matrix's resistance to environmental aggressors. However, the study presents certain limitations: freeze–thaw resistance and sulfate attack were not evaluated, and the long-term stability of phases such as montebrasite remains uncharacterized. These aspects should be addressed in future research through targeted durability tests to comprehensively assess the performance of GGBFS-based binders under aggressive exposure conditions.

Among the newly identified phases, $Bi_{10}Sr_{15}Fe_{10}O_{46}$ stands out as an atypical oxide not commonly associated with cement hydration products. Its presence may be linked to trace-level impurities in the raw materials or to residual phases originating from the slag. While its contribution to the overall matrix performance is likely minimal, its detection highlights the complex mineralogical landscape introduced by GGBFS incorporation and warrants further investigation in future studies.

It is important to note that this study did not assess the heat of hydration or the thermal characteristics of the concrete mixtures containing GGBFS. Given that GGBFS typically reduces the initial heat release due to its slower reaction kinetics compared to Portland cement, the lack of calorimetric or thermal profiling limits a more comprehensive understanding of early-age behavior, especially in massive pours or temperature-sensitive applications. Future investigations should incorporate isothermal calorimetry or semi-adiabatic testing to better characterize the thermal performance and hydration kinetics of GGBFS-modified systems.

4. Discussion

The present study reveals that incorporating GGBFS in high-strength concrete (f'c = 280 kg/cm²) leads to variable effects on mechanical properties that depend on the replacement level and curing conditions. At later ages (28 days), compressive strength is notably enhanced when GGBFS replacement ranges between 16% and 20%, while early-age compressive strength (7 days) can exhibit a slight reduction. This finding aligns with Benkhelil et al. [67], who observed minimal reductions in 7-day compressive strength with GGBFS incorporation, yet reported improvements at 28 days when combined with Portland cement. In contrast, Abdellatief et al. [66] noted that higher replacement ratios may lead to decreased compressive, splitting tensile, and flexural strengths, a trend also reported by Wang et al. [108] and Wang et al. [109].

In terms of tensile performance, our results indicate that a controlled addition of GGBFS can substantially enhance indirect tensile strength. However, Abdellatief et al. [66] found that the splitting tensile strength tends to decline with increased GGBFS, even though a mix with 30% replacement achieved maximum strength at a specific curing age.

The study also demonstrates that partial cement substitution with GGBFS benefits early-age flexural properties, with a moderate replacement level yielding a long-term strength peak. Nevertheless, as reported by Abdellatief et al. [66], flexural strength may diminish at 28 and 90 days when the replacement level is excessively high.

Regarding durability, Kim et al. [68] noted that high-strength early concrete containing up to 30% GGBFS shows lower chloride ion penetration compared to conventional Portland cement concrete. This improved performance is attributed to the refinement of the hydrated matrix microstructure, resulting in reduced porosity and pore size, which corroborates the microstructural findings of this study. Conversely, Sanjuán et al. [22] observed that extremely high GGBFS content (e.g., 62.2%) may increase carbonation depth under short curing periods.

Finally, optimal GGBFS proportions appear to be critical for balancing workability and mechanical performance. Bheel et al. [99] reported that increased dosages of supplementary cementitious materials like GGBFS and metakaolin can reduce workability. If similar workability trends are evident in the current results, these should be discussed alongside the observed improvements in compressive, tensile, and flexural strengths at an optimal 10% binary cementitious dosage, suggesting that a precise balance must be achieved for concrete with f'c = 280 kg/cm².

5. Conclusions

Based on the mechanical results and microstructural findings, which provide a comprehensive insight into the effect of incorporating granulated blast furnace slag (GGBFS) into concrete with f'c = 280 kg/cm², it is concluded that:

- The inclusion of GGBFS, especially at replacement percentages of 16% and 20%, demonstrates a significant increase in 28-day compressive strength compared to the reference concrete.
- Although the indirect tensile strength test showed a decrease at the early stage (7 days) in some cases, a recovery is observed at 28 days, which can be attributed to the latent pozzolanic activity of GGBFS.
- The results of the flexural strength test indicate that the partial substitution of cement with GGBFS enhances flexural properties at early ages. Even though the peak performance at later ages is reached at moderate replacement levels (around 8%), a stable progression in strength evolution is observed.

- The evaluation of the modulus of elasticity confirms an increase in material stiffness, highlighting the stabilizing and reactivating effect of GGBFS in the development of a denser and more homogeneous concrete matrix.
- FTIR analyses reveal that the incorporation of GGBFS causes slight shifts in the absorption bands and an increase in the intensity of peaks associated with functional groups (Si–O and C–O). This indicates an enhancement in the formation of secondary hydration products, such as C-S–H gel, which contribute to matrix densification.
- Morphological studies using SEM and EDS, comparing the reference concrete with that modified by 20% GGBFS, show changes in texture and component distribution. The presence of fibrillar structures and greater heterogeneity in the pores suggest the formation of an interconnected network that improves the internal cohesion of the material.
- X-ray diffraction (XRD) analysis demonstrates a transformation in the mineralogical composition of the concrete, with the emergence of new crystalline phases (such as montebrasite, $Bi_{10}Sr_{15}Fe_{10}O_{46}$, and $BaNiS_2$) and the reduction of phases such as albite and amorphous content. These transformations are consistent with the pozzolanic activity of GGBFS and are related to a potential increase in the durability of the material.
- An optimal selection of the replacement percentage is crucial. The results suggest that, although significant improvements are observed at high substitution levels (16–20%), it is necessary to balance early-age mechanical properties with later-age gains in strength and stiffness.
- The use of Ground Granulated Blast Furnace Slag (GGBFS) as a partial replacement for cement not only enhances the mechanical and microstructural properties of concrete but also provides a sustainable pathway for the valorization of an industrial by-product, contributing to the reduction of CO_2 emissions associated with cement production

6. Declarations

6.1. Author Contributions

Conceptualization, G.C. and E.Y.; methodology, C.B. and A.R.; software, E.Y.; validation, C.B.; formal analysis, A.R.; investigation, G.C., E.Y., and A.R.; resources, G.C.; data curation, G.C.; writing—original draft preparation, C.B.; writing—review and editing, A.R.; visualization, A.R.; supervision, C.B.; project administration, C.B.; funding acquisition, G.C. All authors have read and agreed to the published version of the manuscript.

6.2. Data Availability Statement

The data presented in this study are available on request from the corresponding author.

6.3. Funding

The authors received no financial support for the research, authorship, and/or publication of this article.

6.4. Acknowledgements

We appreciate the support provided by San Juan Bautista Private University during the development of this scientific article.

6.5. Conflicts of Interest

The authors declare no conflict of interest.

7. References

[1] Marvila, M. T., de Azevedo, A. R. G., de Oliveira, L. B., de Castro Xavier, G., & Vieira, C. M. F. (2021). Mechanical, physical and durability properties of activated alkali cement based on blast furnace slag as a function of %Na2O. Case Studies in Construction Materials, 15. doi:10.1016/j.cscm.2021.e00723.

[2] López-Perales, J. F., Contreras, J. E., Vázquez-Rodríguez, F. J., Gómez-Rodríguez, C., Díaz-Tato, L., Banda-Muñoz, F., & Rodríguez, E. A. (2021). Partial replacement of a traditional raw material by blast furnace slag in developing a sustainable conventional refractory castable of improved physical-mechanical properties. Journal of Cleaner Production, 306, 127266. doi:10.1016/j.jclepro.2021.127266.

[3] da Silva, J. M., da Silva, C. E. P., Freire, J. M. A., Becker, H., Diógenes, I. C. N., & Longhinotti, E. (2022). Industrial steel waste-based adsorbent: An effective phosphate removal from aqueous media. Materials Chemistry and Physics, 292, 126828. doi:10.1016/j.matchemphys.2022.126828.

[4] Moula, S., Ben Fraj, A., Wattez, T., Bouasker, M., & Hadj Ali, N. B. (2023). Mechanical properties, carbon footprint and cost of ultra-high performance concrete containing ground granulated blast furnace slag. Journal of Building Engineering, 79, 107796. doi:10.1016/j.jobe.2023.107796.

[5] Roy, A., & Bhattacharya, T. (2022). Ecological and human health risks from pseudo-total and bio-accessible metals in street dusts. Environmental Monitoring and Assessment, 194(2), 101. doi:10.1007/s10661-021-09658-y.

[6] Palod, R., Deo, S. V., & Ramtekkar, G. D. (2020). Effect on mechanical performance, early age shrinkage and electrical resistivity of ternary blended concrete containing blast furnace slag and steel slag. Materials Today: Proceedings, 32, 917–922. doi:10.1016/j.matpr.2020.04.747.

[7] Valipour, M., Yekkalar, M., Shekarchi, M., & Panahi, S. (2014). Environmental assessment of green concrete containing natural zeolite on the global warming index in marine environments. Journal of Cleaner Production, 65, 418–423. doi:10.1016/j.jclepro.2013.07.055.

[8] Serres, N., Braymand, S., & Feugeas, F. (2016). Environmental evaluation of concrete made from recycled concrete aggregate implementing life cycle assessment. Journal of Building Engineering, 5, 24–33. doi:10.1016/j.jobe.2015.11.004.

[9] Bajpai, R., Choudhary, K., Srivastava, A., Sangwan, K. S., & Singh, M. (2020). Environmental impact assessment of fly ash and silica fume based geopolymer concrete. Journal of Cleaner Production, 254, 120147. doi:10.1016/j.jclepro.2020.120147.

[10] Munir, Q., Abdulkareem, M., Horttanainen, M., & Kärki, T. (2023). A comparative cradle-to-gate life cycle assessment of geopolymer concrete produced from industrial side streams in comparison with traditional concrete. Science of the Total Environment, 865, 161230. doi:10.1016/j.scitotenv.2022.161230.

[11] Gerges, N. N., Issa, C. A., Sleiman, E., Aintrazi, S., Saadeddine, J., Abboud, R., & Antoun, M. (2022). Eco-Friendly Optimum Structural Concrete Mix Design. Sustainability (Switzerland), 14(14), 8660. doi:10.3390/su14148660.

[12] Mohamed, A., Zhou, Y., Bertolesi, E., Liu, M., Liao, F., & Fan, M. (2023). Factors influencing self-healing mechanisms of cementitious materials: A review. Construction and Building Materials, 393, 131550. doi:10.1016/j.conbuildmat.2023.131550.

[13] Van Damme, H. (2018). Concrete material science: Past, present, and future innovations. Cement and Concrete Research, 112, 5–24. doi:10.1016/j.cemconres.2018.05.002.

[14] Schneider, M. (2019). The cement industry on the way to a low-carbon future. Cement and Concrete Research, 124(105792). doi:10.1016/j.cemconres.2019.105792.

[15] Monteiro, P. J. M., Miller, S. A., & Horvath, A. (2017). Towards sustainable concrete. Nature Materials, 16(7), 698–699. doi:10.1038/nmat4930.

[16] Flower, D. J. M., & Sanjayan, J. G. (2007). Greenhouse gas emissions due to concrete manufacture. International Journal of Life Cycle Assessment, 12(5), 282–288. doi:10.1065/lca2007.05.327.

[17] Worrell, E., Price, L., Martin, N., Hendriks, C., & Meida, L. O. (2001). Carbon dioxide emissions from the global cement industry. Annual Review of Energy and the Environment, 26, 303–329. doi:10.1146/annurev.energy.26.1.303.

[18] Malhotra, V. M. (2010). Global warming, and role of supplementary cementing materials and superplasticisers in reducing greenhouse gas emissions from the manufacturing of portland cement. International Journal of Structural Engineering, 1(2), 116–130. doi:10.1504/IJSTRUCTE.2010.031480.

[19] Oh, D. Y., Noguchi, T., Kitagaki, R., & Park, W. J. (2014). CO2 emission reduction by reuse of building material waste in the Japanese cement industry. Renewable and Sustainable Energy Reviews, 38, 796–810. doi:10.1016/j.rser.2014.07.036.

[20] Belaidi, A. S. E., Azzouz, L., Kadri, E., & Kenai, S. (2012). Effect of natural pozzolana and marble powder on the properties of self-compacting concrete. Construction and Building Materials, 31, 251–257. doi:10.1016/j.conbuildmat.2011.12.109.

[21] Tung, T. M., Babalola, O. E., & Le, D. H. (2023). Experimental investigation of the performance of ground granulated blast furnace slag blended recycled aggregate concrete exposed to elevated temperatures. Cleaner Waste Systems, 4, 100069. doi:10.1016/j.clwas.2022.100069.

[22] Sanjuán, M. Á., Estévez, E., Argiz, C., & Barrio, D. del. (2018). Effect of curing time on granulated blast-furnace slag cement mortars carbonation. Cement and Concrete Composites, 90, 257–265. doi:10.1016/j.cemconcomp.2018.04.006.

[23] Mohseni, E., Ranjbar, M. M., Yazdi, M. A., Hosseiny, S. S., & Roshandel, E. (2015). The effects of silicon dioxide, iron(III) oxide and copper oxide nanomaterials on the properties of self-compacting mortar containing fly ash. Magazine of Concrete Research, 67(20), 1112–1124. doi:10.1680/macr.15.00051.

[24] Kurad, R., Silvestre, J. D., de Brito, J., & Ahmed, H. (2017). Effect of incorporation of high volume of recycled concrete aggregates and fly ash on the strength and global warming potential of concrete. Journal of Cleaner Production, 166, 485–502. doi:10.1016/j.jclepro.2017.07.236.

[25] Dong, Q., Wang, G., Chen, X., Tan, J., & Gu, X. (2021). Recycling of steel slag aggregate in Portland cement concrete: An overview. Journal of Cleaner Production, 282, 124447. doi:10.1016/j.jclepro.2020.124447.

[26] Miller, S. A. (2018). Supplementary cementitious materials to mitigate greenhouse gas emissions from concrete: can there be too much of a good thing? Journal of Cleaner Production, 178, 587–598. doi:10.1016/j.jclepro.2018.01.008.

[27] Asadollahfardi, G., Katebi, A., Taherian, P., & Panahandeh, A. (2021). Environmental life cycle assessment of concrete with different mixed designs. International Journal of Construction Management, 21(7), 665–676. doi:10.1080/15623599.2019.1579015.

[28] Skibsted, J., & Snellings, R. (2019). Reactivity of supplementary cementitious materials (SCMs) in cement blends. Cement and Concrete Research, 124, 105799. doi:10.1016/j.cemconres.2019.105799.

[29] Thomas, M. D. A., Hooton, R. D., Scott, A., & Zibara, H. (2012). The effect of supplementary cementitious materials on chloride binding in hardened cement paste. Cement and Concrete Research, 42(1), 1–7. doi:10.1016/j.cemconres.2011.01.001.

[30] Siddique, R. (2014). Utilization (recycling) of iron and steel industry by-product (GGBS) in concrete: Strength and durability properties. Journal of Material Cycles and Waste Management, 16(3), 460–467. doi:10.1007/s10163-013-0206-x.

[31] Khatib, J. M., & Hibbert, J. J. (2005). Selected engineering properties of concrete incorporating slag and metakaolin. Construction and Building Materials, 19(6), 460–472. doi:10.1016/j.conbuildmat.2004.07.017.

[32] Yalçınkaya, Ç., & Çopuroğlu, O. (2021). Hydration heat, strength and microstructure characteristics of UHPC containing blast furnace slag. Journal of Building Engineering, 34. doi:10.1016/j.jobe.2020.101915.

[33] Sim, S., Rhee, J. H., Oh, J. E., & Kim, G. (2023). Enhancing the durability performance of thermally damaged concrete with ground-granulated blast furnace slag and fly ash. Construction and Building Materials, 407, 133538. doi:10.1016/j.conbuildmat.2023.133538.

[34] Ganesh, P., & Murthy, A. R. (2019). Tensile behaviour and durability aspects of sustainable ultra-high performance concrete incorporated with GGBS as cementitious material. Construction and Building Materials, 197, 667–680. doi:10.1016/j.conbuildmat.2018.11.240.

[35] Li, Y., Liu, Y., Gong, X., Nie, Z., Cui, S., Wang, Z., & Chen, W. (2016). Environmental impact analysis of blast furnace slag applied to ordinary Portland cement production. Journal of Cleaner Production, 120, 221–230. doi:10.1016/j.jclepro.2015.12.071.

[36] Juenger, M. C. G., Winnefeld, F., Provis, J. L., & Ideker, J. H. (2011). Advances in alternative cementitious binders. Cement and Concrete Research, 41(12), 1232–1243. doi:10.1016/j.cemconres.2010.11.012.

[37] Aydin, S., & Baradan, B. (2014). Effect of activator type and content on properties of alkali-activated slag mortars. Composites Part B: Engineering, 57, 166–172. doi:10.1016/j.compositesb.2013.10.001.

[38] Ahmad, J., Kontoleon, K. J., Majdi, A., Naqash, M. T., Deifalla, A. F., Ben Kahla, N., Isleem, H. F., & Qaidi, S. M. A. (2022). A Comprehensive Review on the Ground Granulated Blast Furnace Slag (GGBS) in Concrete Production. Sustainability (Switzerland), 14(14), 8783. doi:10.3390/su14148783.

[39] Dyavappanavar, S. P., Kulkarni, D. K., Channagoudar, S., Wali, S., Vijapur, G., Patil, S., Sathyanarayana, A., & Shwetha, G. C. (2024). Performance and Evaluation for Durability Enhancement of Self Compacting Concrete Using Ground Granulated Blast Furnace Slag. Journal of Applied Engineering Sciences, 14(2), 236–245. doi:10.2478/jaes-2024-0029.

[40] Gao, D., Yan, D., & Li, X. (2014). Flexural properties after exposure to elevated temperatures of a ground granulated blast furnace slag concrete incorporating steel fibers and polypropylene fibers. Fire and Materials, 38(5), 576–587. doi:10.1002/fam.2198.

[41] Samad, S., Shah, A., & Limbachiya, M. C. (2017). Strength development characteristics of concrete produced with blended cement using ground granulated blast furnace slag (GGBS) under various curing conditions. Sadhana - Academy Proceedings in Engineering Sciences, 42(7), 1203–1213. doi:10.1007/s12046-017-0667-z.

[42] Özbay, E., Erdemir, M., & Durmuş, H. I. (2016). Utilization and efficiency of ground granulated blast furnace slag on concrete properties - A review. Construction and Building Materials, 105, 423–434. doi:10.1016/j.conbuildmat.2015.12.153.

[43] Pal, S. C., Mukherjee, A., & Pathak, S. R. (2003). Investigation of hydraulic activity of ground granulated blast furnace slag in concrete. Cement and Concrete Research, 33(9), 1481–1486. doi:10.1016/S0008-8846(03)00062-0.

[44] Yeau, K. Y., & Kim, E. K. (2005). An experimental study on corrosion resistance of concrete with ground granulate blast-furnace slag. Cement and Concrete Research, 35(7), 1391–1399. doi:10.1016/j.cemconres.2004.11.010.

[45] Sharma, A. K., & Sivapullaiah, P. V. (2016). Ground granulated blast furnace slag amended fly ash as an expansive soil stabilizer. Soils and Foundations, 56(2), 205–212. doi:10.1016/j.sandf.2016.02.004.

[46] Dinakar, P., Sethy, K. P., & Sahoo, U. C. (2013). Design of self-compacting concrete with ground granulated blast furnace slag. Materials and Design, 43, 161–169. doi:10.1016/j.matdes.2012.06.049.

[47] Abbass, M., Singh, D., & Singh, G. (2021). Properties of hybrid geopolymer concrete prepared using rice husk ash, fly ash and GGBS with coconut fiber. Materials Today: Proceedings, 45, 4964–4970. doi:10.1016/j.matpr.2021.01.390.

[48] Liu, X., Xiao, G., Yang, D., Dai, L., & Tang, A. (2024). Sustainable Cementitious Materials: Strength and Microstructural Characteristics of Calcium Carbide Residue-Activated Ground Granulated Blast Furnace Slag–Fly Ash Composites. Sustainability (Switzerland), 16(24), 11168. doi:10.3390/su162411168.

[49] Naik, T. R. (2008). Sustainability of Concrete Construction. Practice Periodical on Structural Design and Construction, 13(2), 98–103. doi:10.1061/(asce)1084-0680(2008)13:2(98).

[50] Crossin, E. (2015). The greenhouse gas implications of using ground granulated blast furnace slag as a cement substitute. Journal of Cleaner Production, 95, 101–108. doi:10.1016/j.jclepro.2015.02.082.

[51] Zhao, H., Sun, W., Wu, X., & Gao, B. (2015). The properties of the self-compacting concrete with fly ash and ground granulated blast furnace slag mineral admixtures. Journal of Cleaner Production, 95, 66–74. doi:10.1016/j.jclepro.2015.02.050.

[52] Yu, R., Spiesz, P., & Brouwers, H. J. H. (2015). Development of an eco-friendly Ultra-High Performance Concrete (UHPC) with efficient cement and mineral admixtures uses. Cement and Concrete Composites, 55, 383–394. doi:10.1016/j.cemconcomp.2014.09.024.

[53] Gholampour, A., & Ozbakkaloglu, T. (2017). Performance of sustainable concretes containing very high volume Class-F fly ash and ground granulated blast furnace slag. Journal of Cleaner Production, 162, 1407–1417. doi:10.1016/j.jclepro.2017.06.087.

[54] Verian, K. P., Ashraf, W., & Cao, Y. (2018). Properties of recycled concrete aggregate and their influence in new concrete production. Resources, Conservation and Recycling, 133, 30–49. doi:10.1016/j.resconrec.2018.02.005.

[55] Prasanna, P. K., Srinivasu, K., & Ramachandra Murthy, A. (2021). Strength and durability of fiber reinforced concrete with partial replacement of cement by Ground Granulated Blast Furnace Slag. Materials Today: Proceedings, 47, 5416–5425. doi:10.1016/j.matpr.2021.06.267.

[56] Cahyani, R. A. T., & Rusdianto, Y. (2021). An Overview of Behaviour of Concrete with Granulated Blast Furnace Slag as Partial Cement Replacement. IOP Conference Series: Earth and Environmental Science, 933(1), 012006. doi:10.1088/1755-1315/933/1/012006.

[57] Liu, S., Wang, Z., & Li, X. (2014). Long-term properties of concrete containing ground granulated blast furnace slag and steel slag. Magazine of Concrete Research, 66(21), 1095–1103. doi:10.1680/macr.14.00074.

[58] Majhi, R. K., & Nayak, A. N. (2019). Bond, durability and microstructural characteristics of ground granulated blast furnace slag based recycled aggregate concrete. Construction and Building Materials, 212, 578–595. doi:10.1016/j.conbuildmat.2019.04.017.

[59] Kim, H., Koh, T., & Pyo, S. (2016). Enhancing flowability and sustainability of ultra-high performance concrete incorporating high replacement levels of industrial slags. Construction and Building Materials, 123, 153–160. doi:10.1016/j.conbuildmat.2016.06.134.

[60] Chen, H. J., Huang, S. S., Tang, C. W., Malek, M. A., & Ean, L. W. (2012). Effect of curing environments on strength, porosity and chloride ingress resistance of blast furnace slag cement concretes: A construction site study. Construction and Building Materials, 35, 1063–1070. doi:10.1016/j.conbuildmat.2012.06.052.

[61] Divsholi, B. S., Lim, T. Y. D., & Teng, S. (2014). Durability Properties and Microstructure of Ground Granulated Blast Furnace Slag Cement Concrete. International Journal of Concrete Structures and Materials, 8(2), 157–164. doi:10.1007/s40069-013-0063-y.

[62] Cao, Q., Nawaz, U., Jiang, X., Zhanga, L., & Ansari, W. S. (2022). Effect of air-cooled blast furnace slag aggregate on mechanical properties of ultra-high-performance concrete. Case Studies in Construction Materials, 16. doi:10.1016/j.cscm.2022.e01027.

[63] Jose, S. K., Soman, M., & Sheela Evangeline, Y. (2021). Ecofriendly building blocks using foamed concrete with ground granulated blast furnace slag. International Journal of Sustainable Engineering, 14(4), 776-784. doi:10.1080/19397038.2020.1836064.

[64] Song, W., Zhu, Z., Pu, S., Wan, Y., Huo, W., Song, S., Zhang, J., Yao, K., & Hu, L. (2020). Efficient use of steel slag in alkali-activated fly ash-steel slag-ground granulated blast furnace slag ternary blends. Construction and Building Materials, 259, 119814. doi:10.1016/j.conbuildmat.2020.119814.

[65] Tang, Z., Li, W., Tam, V. W. Y., & Luo, Z. (2020). Investigation on dynamic mechanical properties of fly ash/slag-based geopolymeric recycled aggregate concrete. Composites Part B: Engineering, 185, 107776. doi:10.1016/j.compositesb.2020.107776.

[66] Abdellatief, M., AL-Tam, S. M., Elemam, W. E., Alanazi, H., Elgendy, G. M., & Tahwia, A. M. (2023). Development of ultra-high-performance concrete with low environmental impact integrated with metakaolin and industrial wastes. Case Studies in Construction Materials, 18. doi:10.1016/j.cscm.2022.e01724.

[67] Benkhelil, M., Arroudj, K., Guettala, S., & Douara, T. H. (2023). Prediction of the physico-mechanical characteristics of a high-performance concrete containing dune sand powder and ground blast-furnace slag. Construction and Building Materials, 398, 132482. doi:10.1016/j.conbuildmat.2023.132482.

[68] Kim, Y., Hanif, A., Usman, M., Munir, M. J., Kazmi, S. M. S., & Kim, S. (2018). Slag waste incorporation in high early strength concrete as cement replacement: Environmental impact and influence on hydration & durability attributes. Journal of Cleaner Production, 172, 3056–3065. doi:10.1016/j.jclepro.2017.11.105.

[69] Moula, S., Ben Fraj, A., Wattez, T., Bouasker, M., & Bel Hadj Ali, N. (2023). The very early-age behaviour of Ultra-High Performance Concrete containing ground granulated blast furnace slag. Construction and Building Materials, 400. doi:10.1016/j.conbuildmat.2023.132630.

[70] Su, N., Hsu, K. C., & Chai, H. W. (2001). A simple mix design method for self-compacting concrete. Cement and Concrete Research, 31(12), 1799–1807. doi:10.1016/S0008-8846(01)00566-X.

[71] Cahyani, R. A. T., Setyono, E., & Rusdianto, Y. (2020). Performa Beton Dengan Ground Granulated Blast Furnace Slag Terhadap Sulfate Attack. Jurnal Rekayasa Sipil (JRS-Unand), 16(3), 185. doi:10.25077/jrs.16.3.185-193.2020.

[72] Cahyani, R. A. T., & Rusdianto, Y. (2020). Concrete Performance with Ground Granulated Blast Furnace Slag as Supplementary Cementitious Materials. IOP Conference Series: Materials Science and Engineering, 771(1), 012062. doi:10.1088/1757-899X/771/1/012062.

[73] Lee, J. Y., Choi, J. S., Yuan, T. F., Yoon, Y. S., & Mitchell, D. (2019). Comparing properties of concrete containing electric arc furnace slag and granulated blast furnace slag. Materials, 12(9), 1371. doi:10.3390/ma12091371.

[74] Ustabaş, İ., & Kaya, A. (2018). Comparing the pozzolanic activity properties of obsidian to those of fly ash and blast furnace slag. Construction and Building Materials, 164, 297–307. doi:10.1016/j.conbuildmat.2017.12.185.

[75] Lal Jain, K., Singh Rajawat, L., & Sancheti, G. (2021). Mechanical Properties of Ground Granulated Blast Furnace Slag Made Concrete. IOP Conference Series: Earth and Environmental Science, 796(1), 012063. doi:10.1088/1755-1315/796/1/012063.

[76] Malipeddi, R., & Adiseshu, S. (2022). Ground Granulated Blast Furnace Slag as a Cement Replacement in Concrete: An Analysis of Dissolution. Journal of The Institution of Engineers (India): Series A, 103(2), 481–492. doi:10.1007/s40030-022-00623-7.

[77] Patra, R. K., & Mukharjee, B. B. (2017). Influence of incorporation of granulated blast furnace slag as replacement of fine aggregate on properties of concrete. Journal of Cleaner Production, 165, 468–476. doi:10.1016/j.jclepro.2017.07.125.

[78] Patra, R. K., & Mukharjee, B. B. (2024). Characteristics of concrete containing granulated blast furnace slag: a factorial design approach. Journal of Building Pathology and Rehabilitation, 9(1), 73. doi:10.1007/s41024-024-00429-z.

[79] Mukharjee, B. B., & Patra, R. K. (2021). Effects of utilising granulated blast furnace slag as fine aggregate on concrete: a factorial design approach. Innovative Infrastructure Solutions, 6(4), 195. doi:10.1007/s41062-021-00565-2.

[80] Oseke, I. F., & Dangiwa, F. P. (2025). Optimal Cement Replacement Levels in Concrete Using Ground Granulated Blast Furnace-Slag for Workability and Strength Development. Open Journal of Engineering Science, 6(1), 1–14. doi:10.52417/ojes.v6i1.786.

[81] Vishakha N. Surati, V. N. S. (2022). Application of Ground Granulated Blast Furnace Slag (GGBS) In High Performance Concrete. Journal of Science and Technology, 7(9), 12–23. doi:10.46243/jst.2022.v7.i09.pp12-23.

[82] Sahu, A., Kumar, S., Srivastav, A., & Anurag, H. (2025). Experimental investigation on the performance of ground granulated blast furnace slag and copper slag blended recycled aggregate concrete exposed to elevated temperatures. Journal of Building Engineering, 105(112531). doi:10.1016/j.jobe.2025.112531.

[83] Shen, D., Jiao, Y., Gao, Y., Zhu, S., & Jiang, G. (2020). Influence of ground granulated blast furnace slag on cracking potential of high performance concrete at early age. Construction and Building Materials, 241, 117839. doi:10.1016/j.conbuildmat.2019.117839.

[84] Manojsuburam, R., Sakthivel, E., & Jayanthimani, E. (2022). A study on the mechanical properties of alkali activated ground granulated blast furnace slag and fly ash concrete. Materials Today: Proceedings, 62, 1761–1764. doi:10.1016/j.matpr.2021.12.328.

[85] Tran, T. M., Trinh, H. T. M. K., Nguyen, D., Tao, Q., Mali, S., & Pham, T. M. (2023). Development of sustainable ultra-high-performance concrete containing ground granulated blast furnace slag and glass powder: Mix design investigation. Construction and Building Materials, 397, 132358. doi:10.1016/j.conbuildmat.2023.132358.

[86] Sumajouw, D. M. J., Hardjito, D., Wallah, S. E., & Rangan, B. V. (2007). Fly ash-based geopolymer concrete: Study of slender reinforced columns. Journal of Materials Science, 42(9), 3124–3130. doi:10.1007/s10853-006-0523-8.

[87] Siddique, R., & Kunal. (2016). Utilization of industrial by-products and natural ashes in mortar and concrete. Nonconventional and Vernacular Construction Materials, 159–204. doi:10.1016/b978-0-08-100038-0.00007-x.

[88] Tahwia, A. M., Elgendy, G. M., & Amin, M. (2022). Mechanical properties of affordable and sustainable ultra-high-performance concrete. Case Studies in Construction Materials, 16. doi:10.1016/j.cscm.2022.e01069.

[89] Althoey, F., Ansari, W. S., Sufian, M., & Deifalla, A. F. (2023). Advancements in low-carbon concrete as a construction material for the sustainable built environment. Developments in the Built Environment, 16, 100284. doi:10.1016/j.dibe.2023.100284.

[90] Fode, T. A., Chande Jande, Y. A., & Kivevele, T. (2023). Effects of different supplementary cementitious materials on durability and mechanical properties of cement composite-Comprehensive review. Heliyon, 9(7), e17924. doi:10.1016/j.heliyon.2023.e17924.

[91] Dellinghausen, L. M., Gastaldini, A. L. G., Vanzin, F. J., & Veiga, K. K. (2012). Total shrinkage, oxygen permeability, and chloride ion penetration in concrete made with white Portland cement and blast-furnace slag. Construction and Building Materials, 37, 652–659. doi:10.1016/j.conbuildmat.2012.07.076.

[92] Yuan, J., Lindquist, W., Darwin, D., & Browning, J. A. (2015). Effect of slag cement on drying shrinkage of concrete. ACI Materials Journal, 112(2), 267–276. doi:10.14359/51687129.

[93] Zhou, X. M., Slater, J. R., Wavell, S. E., & Oladiran, O. (2012). Effects of PFA and GGBS on early-ages engineering properties of Portland cement systems. Journal of Advanced Concrete Technology, 10(2), 74–85. doi:10.3151/jact.10.74.

[94] Sara, B., Mhamed, A., Otmane, B., & Karim, E. (2023). Elaboration of a Self-Compacting mortar based on concrete demolition waste incorporating blast furnace slag. Construction and Building Materials, 366. doi:10.1016/j.conbuildmat.2022.130165.

[95] Mehta, A., Siddique, R., Ozbakkaloglu, T., Uddin Ahmed Shaikh, F., & Belarbi, R. (2020). Fly ash and ground granulated blast furnace slag-based alkali-activated concrete: Mechanical, transport and microstructural properties. Construction and Building Materials, 257. doi:10.1016/j.conbuildmat.2020.119548.

[96] ASTM C136/C136M-19. (2019). Standard Test Method for Sieve Analysis of Fine and Coarse Aggregates. ASTM International, Pennsylvania, United States. doi:10.1520/C0136_C0136M-19.

[97] ACI 211.1-91. (2002) Standard Practice for Selecting Proportion Normal, Heavyweight and Mass Concrete. American Concrete Institute (ACI), Farmington Hills, United States.

[98] ASTM C192/C192M-19. (2024). Standard Practice for Making and Curing Concrete Test Specimens in the Laboratory. ASTM International, Pennsylvania, United States. doi:10.1520/C0192_C0192M-19.

[99] Bheel, N., Abbasi, S. A., Awoyera, P., Olalusi, O. B., Sohu, S., Rondon, C., & Echeverriá, A. M. (2020). Fresh and hardened properties of concrete incorporating binary blend of metakaolin and ground granulated blast furnace slag as supplementary cementitious material. Advances in Civil Engineering, 8851030. doi:10.1155/2020/8851030.

[100] Qi, A., Liu, X., Wang, Z., & Chen, Z. (2020). Mechanical properties of the concrete containing ferronickel slag and blast furnace slag powder. Construction and Building Materials, 231. doi:10.1016/j.conbuildmat.2019.117120.

[101] ASTM C39/C39M-18. (2003). Standard Test Method for Compressive Strength of Cylindrical Concrete Specimens. ASTM International, Pennsylvania, United States. doi:10.1520/C0039_C0039M-18.

[102] ASTM C496/C496M-17. (2017). Standard Test Method for Splitting Tensile Strength of Cylindrical Concrete Specimens. ASTM International, Pennsylvania, United States. doi:10.1520/C0496_C0496M-17.

[103] ASTM C293/C293M-16. (2010). Standard Test Method for Flexural Strength of Concrete (Using Simple Beam With Center-Point Loading) (Withdrawn 2025). ASTM International, Pennsylvania, United States.

[104] ASTM C469/C469M-22. (2022). Standard Test Method for Static Modulus of Elasticity and Poisson's Ratio of Concrete in Compression. ASTM International, Pennsylvania, United States.

[105] ASTM E1252-98(2021). (2021). Standard Practice for General Techniques for Obtaining Infrared Spectra for Qualitative Analysis. ASTM International, Pennsylvania, United States. doi:10.1520/E1252-98R21.

[106] ASTM C1723-16. (2022). Standard Guide for Examination of Hardened Concrete Using Scanning Electron Microscopy. ASTM International, Pennsylvania, United States. doi:10.1520/C1723-16.

[107] UNE-EN 13925-1:2006. (2006). Non-Destructive Testing—X-ray Diffraction from Polycrystalline and Amorphous Materials—Part 1: General Principles. AENOR (Asociación Española de Normalización), Madrid, Spain.

[108] Wang, J. L., Niu, K. M., Yang, Z. F., Zhou, M. K., Sun, L. Q., & Ke, G. J. (2009). Effects of fly ash and ground granulated blast-furnaces slag on properties of high-strength concrete. Key Engineering Materials, 405–406, 219–225. doi:10.4028/www.scientific.net/kem.405-406.219.

[109] Wang, Q., Yan, P., Yang, J., & Zhang, B. (2013). Influence of steel slag on mechanical properties and durability of concrete. Construction and Building Materials, 47, 1414–1420. doi:10.1016/j.conbuildmat.2013.06.044.